

# A multifunctional additive strategy to stabilize the precursor solution and passivate film defects for MA-free perovskite solar cells with an efficiency of 22.75%



Huan Bi <sup>a, b</sup>, Mengna Guo <sup>a</sup>, Chao Ding <sup>b</sup>, Shuzi Hayase <sup>b</sup>, Qing Shen <sup>b, \*</sup>, Gaoyi Han <sup>a, \*\*</sup>, Wenjing Hou <sup>a, \*\*\*</sup>

<sup>a</sup> Institute of Molecular Science, Key Laboratory of Materials for Energy Conversion and Storage of Shanxi Province, Shanxi University, Taiyuan 030006, PR China

<sup>b</sup> Faculty of Informatics and Engineering, The University of Electro-Communications, 1-5-1 Chofugaoka, Chofu, Tokyo 182-8585, Japan

## ARTICLE INFO

### Article history:

Received 25 October 2022  
Received in revised form  
3 February 2023  
Accepted 17 February 2023  
Available online 24 February 2023

### Keywords:

Reduce  $I_2$   
Ion migration suppression  
Defect passivation  
Weak interaction  
Benzoyl hydrazine

## ABSTRACT

Though great progress has been realized in perovskite solar cells (PSCs), there are still some thorny challenges that exist such as 1) low power conversion efficiency (PCE) and loss of stability due to the defects in the film; 2) poor reproducibility of solution-processed PSCs due to the unstable perovskite precursor solution. Here, an effective multifunctional additive, benzoyl hydrazine (BH), was developed to modify the perovskite film. The result shows that the defect of the film decreased after BH modification due to the interaction between BH and perovskite. Meanwhile, the I ions ( $I^-$ ) migration is also suppressed due to the weak interaction between BH and perovskite. In addition, the  $-NH-NH_2$  in BH can reduce the undesired  $I_2$  by reducing it to  $I^-$ . Finally, the PCE of PSCs modified by BH achieved a PCE of 22.75%, which is one of the highest PCE of the reported MA-free PSCs. The modified device still exhibited excellent stability in different conditions.

© 2023 Elsevier Ltd. All rights reserved.

## 1. Introduction

Since the first perovskite solar cells (PSCs) invented by Miyasaka in 2009, PSCs have entered a golden age of development [1] due to its excellent optoelectronic properties such as a long carrier lifetime, tunable bandgap, high molar absorption coefficient, long carrier diffusion length, and so on [2–5]. Up to now, the certified power conversion efficiency (PCE) of a single junction has achieved 25.7%, which is an unprecedented achievement in the photovoltaic field [6]. Although a high PCE has been obtained in PSCs, poor stability still hinders the commercialization of PSCs. The composition of the perovskite light-absorbing layer is closely related to the performance of PSC devices. At present, most high-efficiency PSCs (PCE > 24%) are based on MA-based mixed cation perovskite films (such as MAFA, MAFACs, etc.). However, the stability of MA-based

PSCs is very poor, which is mainly due to the easy escape of MA from the lattice once heated, thereby destroying the film structure [7]. In addition, the extremely easy phase transition also makes MA-based PSCs an obstacle to the commercialization of PSCs [8–10]. Therefore, it is urgent to develop MA-free PSCs. Actually, as we previously reported, systematic optimization on MA-free PSCs has been conducted. And our previous results reveal that the device based on the MA-free perovskite composition ( $Rb_{0.02}(FA_{0.95}Cs_{0.05})_{0.98}PbI_{2.91}Br_{0.03}Cl_{0.06}$ ) exhibited the highest efficiency. Hence, the perovskite composition ( $Rb_{0.02}(FA_{0.95}Cs_{0.05})_{0.98}PbI_{2.91}Br_{0.03}Cl_{0.06}$ ) was employed for further investigation in the present work.

It is well-known that a sea of defects could be generated due to the rapid crystallizing and growth of the film, which would seriously damage the quality of the film, PSCs' PCE, and stability [11,12]. So far, a lot of strategies have been developed to reduce the defects of the film, such as perovskite composition engineering, precursor solvent, antisolvent engineering, additive engineering, deposition substrate modulation, etc. [11–14]. Among them, additive engineering has been widely regarded as an effective strategy to improve the quality of the film because not only can it reduce the defects of the film but also can change the precursor solution

\* Corresponding author.

\*\* Corresponding author.

\*\*\* Corresponding author.

E-mail addresses: [shen@pc.uec.ac.jp](mailto:shen@pc.uec.ac.jp) (Q. Shen), [han\\_gaoyi@sxu.edu.cn](mailto:han_gaoyi@sxu.edu.cn) (G. Han), [houwening@sxu.edu.cn](mailto:houwening@sxu.edu.cn) (W. Hou).

properties. Wang and his co-workers developed a new additive name  $K_2SO_4$ , the ultrathin GB passivation layer is in situ constructed. Finally, a PCE of 22.40% was achieved and the device showed competitive stability [15]. Ma's group also improved the PCE of PSCs by introducing a multifunction additive [16]. However, only a few workers focus their eyes on MA-free PSCs; consequently, it is imperative to develop novel multifunctional additives for improving the efficiency and stability of MA-free PSCs.

Besides, preventing I<sup>-</sup> ions migration and controlling the properties of the precursor solution are another key factors to improve the PCE and stability of the PSCs. As is known to all that I<sup>-</sup> migration is unavoidable and can cause an accelerated device failure, notorious hysteresis factors, reduced device efficiency, and so on [17–19]. So how to suppress I<sup>-</sup> migration is important. Some works have been done to inhibit I<sup>-</sup> migration [20,21], such as introducing an interface modifier or additive [22–24]. Among them, employing an additive is helpful to suppress I<sup>-</sup> migration at the interface or in the bulk. In addition, the placed precursor solution also produces an ionic agglomeration to generate I<sub>2</sub>, which is also harmful to PSCs. Some work attempted to reduce the generation of I<sub>2</sub> by preparing the precursor solution when using rather than standing for a long time [2,17,25–27]. However, such a mysterious chemical reaction cannot be improved only from the process but needs to be explored from the root. Therefore, it is necessary to find a suitable reducing agent to promote the reduction of I<sub>2</sub> and suppress the I<sup>-</sup> migration.

In this work, a new-type of multifunctional additive (benzoyl hydrazine, BH) was adopted to improve the PCE and stability of the PSCs. After modification, the defects of the film were reduced significantly; meanwhile, the film thickness and the grain size were

increased. In addition, the migration of I<sup>-</sup> is significantly inhibited. Besides, the –NH–NH<sub>2</sub> in BH can reduce the I<sub>2</sub> to I<sup>-</sup>, thereby inhibiting the generation of I<sub>2</sub> in the precursor solution. As a result, both PCE and stability are improved after BH modification. The PSCs modified by BH get a PCE of 22.75%. The unencapsulated modified device maintains 98% of its initial PCE after aging in air and dark conditions for 500 h, 94.6% of its original PCE after aging in air conditions with a relative humidity of 40–50% for 300 h, and 96.8% of its initial PCE in comprehensive conditions, respectively. This work provides a simple and effective strategy to stabilize the precursor solution and passivate the defects, which paves the way for the industrialization of perovskite photovoltaic technology.

## 2. Result and discussion

The structure of the PSCs employed in the present work is displayed in Fig. 1a (FTO/TiO<sub>2</sub>/perovskite/Spiro-OMeTAD/Ag), where the composition of the perovskite (PVSK) is  $Rb_{0.02}(FA_{0.95}Cs_{0.05})_{0.98}PbI_{2.91}Br_{0.03}Cl_{0.06}$ . The electronic static potential of BH is exhibited in Fig. 1b, as we can see that a dense electron cloud was formed around O of –C=O. Meanwhile, the Milliken charge distribution is calculated and displayed in Fig. 1c, which is the same as for the electronic static potential. In order to uncover the chemical interaction between BH and PVSK, X-ray photoelectron spectroscopy (XPS) measurement was employed. Fig. S1 shows the full XPS spectra of the PVSK, BH, and PVSK + BH. As shown in Fig. 1d, Pb 4f<sub>7/2</sub> and Pb 4f<sub>5/2</sub> peaks were shifted from 138.28 eV to 143.17 eV of the pristine film to 137.91 eV and 142.78 eV of the target film [28]. It is well known that the lower binding energy indicates more electrons clustered around the

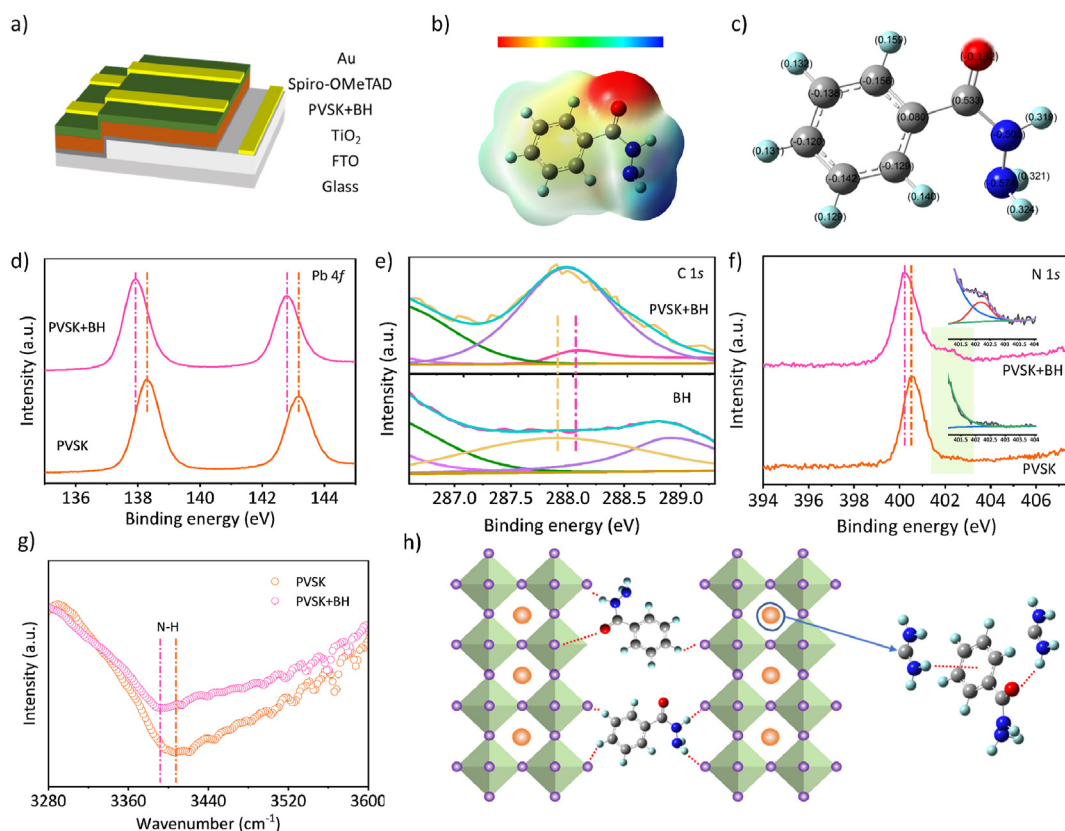


**Fig. 1.** (a) A schematic illustration of the architecture of the perovskite solar cell in this work. (b) electronic static potential and (c) Milliken charge distribution of the benzoyl hydrazine. X-ray photoelectron spectroscopy (d) Pb 4f, (e) C 1s, and (f) N 1s core-level spectra of control and target perovskite films as well as pure benzoyl hydrazine. (g) Fourier transform infrared spectroscopy spectra of the control and target perovskite film. (h) Schematically illustrated a defect passivation and ion migration inhibition mechanism.

element, which suggests that there is a strong chemical interaction between PVS<sub>K</sub> and BH. In addition, the peak located at 287.91 eV of the BH is assigned to C 1s on the benzene ring [29,30]. After mixing with the PVS<sub>K</sub>, the binding energy of C 1s was shifted to 288.03 eV. A significantly shifted binding energy of C 1s indicates that there is a strong chemical interaction between the benzene ring and PVS<sub>K</sub>. Further, the shift of N 1s also gives evidence of chemical interaction between BH and PVS<sub>K</sub>. Fig. S1d shows the XPS result of I 3d for the perovskite films treated with or without BH. Compared with the control film, the peak position shifted towards the lower binding energy for the target film, which suggested that a strong chemical interaction exists between perovskite (I<sup>-</sup>) and BH [31]. In addition, for the control film, an obvious peak located at 619 eV was assigned to I<sub>2</sub> [32], while this peak can't be observed in the target film, which proves that the I<sub>2</sub> was reduced after introducing BH.

A Fourier transform infrared spectroscopy measurement was carried out to further study the chemical interaction between the additive and perovskites. As exhibited in Fig. 1g, the stretching vibration peak of -N-H in PVS<sub>K</sub> at 3407 cm<sup>-1</sup> was shifted to a low

wavenumber of 3392 cm<sup>-1</sup> for the BH-treated perovskite film, which can be considered as a hydrogen bond formed between BH and PVS<sub>K</sub> [33], which is consistent with the result of XPS. Fig. 1h schematically illustrates the interaction between BH and perovskite. As we can see that BH can passivate the Pb defect by coordination roles between -C=O and Pb<sup>2+</sup>. The undercoordinated Pb<sup>2+</sup> defects are always formed in the perovskite film when the X-site in ABX<sub>3</sub> is missing. The previous reports have illustrated that the O in -C=O has lone pair electrons [34–36], which will coordinate with Pb<sup>2+</sup> by donating electrons to the empty orbital of Pb. Besides, BH can also suppress the I<sup>-</sup> migration by -N-H...I and limit the cation rotation through weak interactions of -C=O...H-N- and N-H...benzene.

Top-view scanning electron microscopy technology was further employed to uncover the effect of BH modification on the morphology of the control and target perovskite film, as illustrated in Fig. 2a and b. It can be seen clearly that the grain size of the target film increased compared with the control film. Fig. S2 shows the grain size statistics, the average grain size increased to around

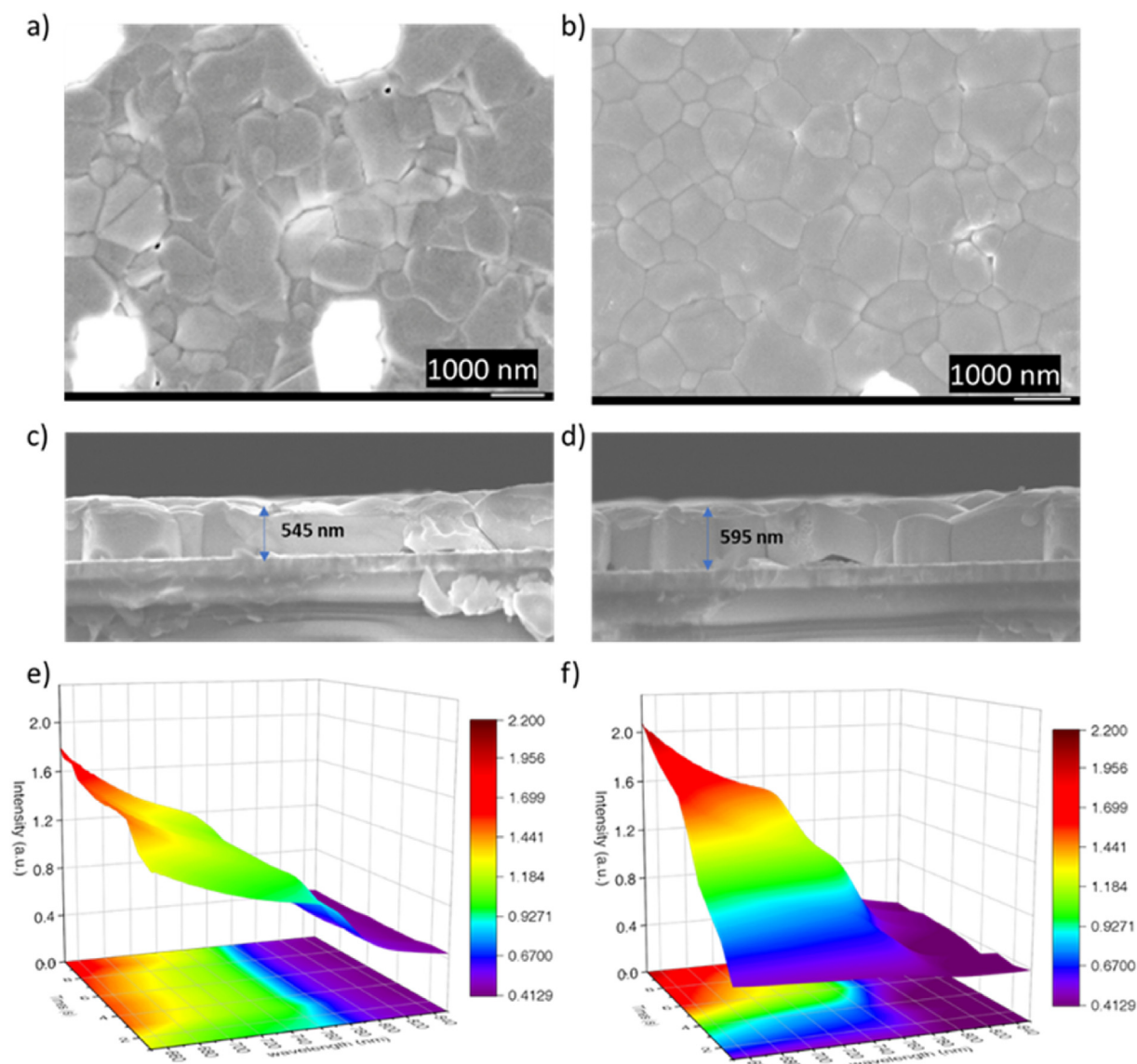
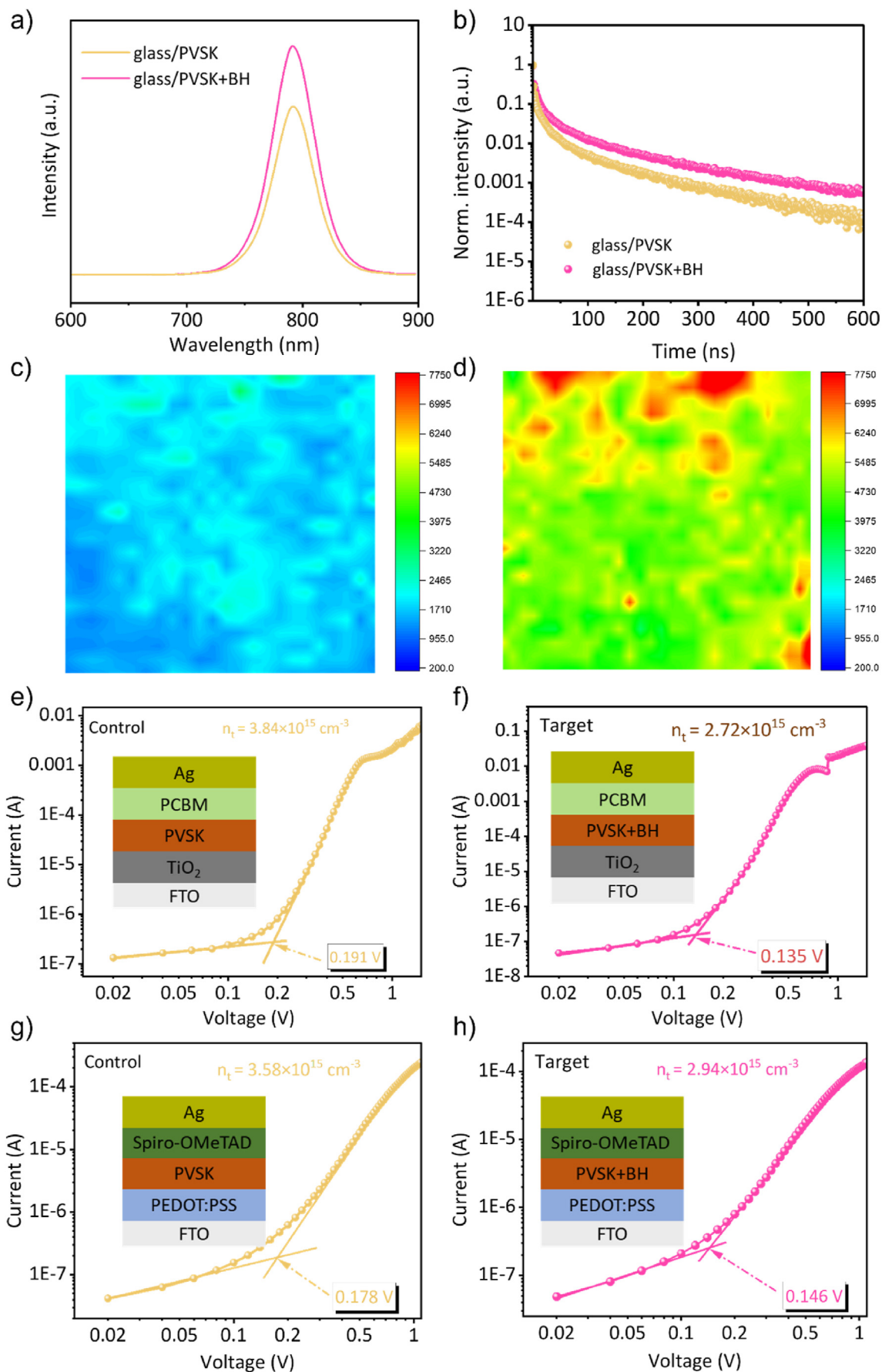


**Fig. 2.** Top-view scanning electron microscopy images of the (a) control and (b) target perovskite films. Cross-section scanning electron microscopy of the (c) control and (d) target perovskite films. Time-resolved ultraviolet–visible spectroscopy of the film (e) without (545 nm) and (f) with benzoyl hydrazin modification (595 nm).



1066 nm, while the control film was only around 903 nm. A cross-section scanning electron microscopy image indicated that the thickness of the thin film was increased after the BH modification (Fig. 2c and d), which may cause the device with a high current. To uncover the reason for the increased grain size and film thickness, time-resolved ultraviolet–visible (UV–vis) spectroscopy was carried out. As presented in Fig. 2e and f (2D result illustrated in Fig. S3), after spinning, the film is placed on a hot plate to anneal at 130 °C. As we can see that the perovskite film formed immediately without the BH modification, while the target perovskite film did not. The time-resolved UV–vis result indeed suggests that BH can delay the formation of perovskite films, and this would lead to a larger grain.

Steady-state photoluminescence (PL) and time-resolved PL (TRPL) spectra were collected to gain insights into the defects in perovskite films without and with BH modification with a structure of a glass/perovskite. As revealed from the PL spectra in Fig. 3a, the much increased PL intensity is realized after introducing BH, which can be attributed to the improved film quality with reduced defects by BH modification. TRPL spectra was fitted well with the following equation [26,27].

$$I(t) = A_1 e^{-\frac{t}{\tau_1}} + A_2 e^{-\frac{t}{\tau_2}}$$

where,  $\tau_1$  and  $\tau_2$  correspond to the fast and slow decay time constant, respectively.  $A_1$  and  $A_2$  are the amplitude of the fast and slow decay processes, respectively. The average carrier lifetime ( $\tau_{ave}$ ) can be calculated via the following equation [26,27]:

$$\tau_{ave} = \frac{A_1 \tau_1^2 + A_2 \tau_2^2}{A_1 \tau_1 + A_2 \tau_2}$$

The fitting results are displayed in Table S1. The average photoexcited carrier lifetime of the target perovskite film was increased (108.20 ns) compared with the pristine film (64.49 ns). This result suggested that the defect density of the perovskite film was reduced after introducing BH in the perovskite solution. The reduced defect can own to the strong chemical interaction between BH and perovskite, which can passivate the defect of the perovskite (such as the undercoordinated  $Pb^{2+}$ ). On the other hand, the slow crystallization process also favors the formation of higher quality films. In addition, PL mapping images show the same trend as the PL curves (Fig. 3c and d). Space charge limited current measurements were further employed to investigate the defect density in the perovskite film. Fig. 3e and f display the dark  $J$ - $V$  curves of electron-only devices with the structure of FTO/TiO<sub>2</sub>/PVSK or PVSK + BH/PCBM/Ag. It is well known that the defect density could be calculated according to the equation of  $n_t = (2\epsilon\epsilon_0 V_{TFL})/(eL^2)$  [37], where  $\epsilon$  is the dielectric constant of the perovskite,  $\epsilon_0$  is the vacuum dielectric constant,  $V_{TFL}$  is the trap-filled limit voltage obtained by fitting dark  $J$ - $V$  curves,  $L$  is the thickness film of the perovskite, and  $e$  is the elementary charge. The  $V_{TFL}$  of the electron-only devices with and without BH is 0.191 V and 0.135 V, respectively, resulting in the decreased trap density  $n_t$  from  $3.84 \times 10^{15} \text{ cm}^{-3}$  to  $2.72 \times 10^{15} \text{ cm}^{-3}$ , which was consistent with the increased PL intensity and carrier lifetimes. Besides, hole-only devices with the structure of FTO/PEDOT:PSS/PVSK or PVSK + BH/Spiro-OMeTAD/Ag were also fabricated to uncover the defects in the film. Being the same as the electron-only devices, the  $V_{TFL}$  of the hole-only device

without and with BH is 0.178 V and 0.146 V, respectively, resulting in the decreased trap density  $n_t$  from  $3.58 \times 10^{15} \text{ cm}^{-3}$  to  $2.94 \times 10^{15} \text{ cm}^{-3}$ . The improved film quality can be attributed to the following reasons: first, the strong coordination between  $-C=O$  and under coordination  $Pb^{2+}$  could reduce the anionic defects in the perovskite films. Second, the hydrogen bond between I and  $-NH$  ( $-NH\dots I$ ) inhibits the migration of I, thereby reducing the I vacancy defects in the film. Third, the  $FA^+$  or  $MA^+$  vacancies may be reduced due to the effective inhibition of organic cation migration by forming a strong hydrogen bond between BH and  $NH_3^+$ .

Electrochemical impedance spectroscopy was carried out to help us further uncover the dynamics of interfacial charge extraction in devices without or with BH modification. Fig. 4a exhibits the Nyquist plots of the PSCs without and with BH modification measured at a bias of 0 V in the frequency range of 1 MHz to 0.1 Hz under dark conditions. It was reported that the semicircle in the high-frequency region is related to charge-transfer resistance ( $R_{ct}$ ) and the incomplete semicircle in the low-frequency region is associated with recombination resistance ( $R_{rec}$ ) [26,28,38]. After introducing BH into the perovskite film, the  $R_{ct}$  was reduced, mainly, because of the increased grain size and reduced grain boundary. On the other hand, the  $R_{rec}$  was increased, which can be attributed to the reduced defects and increased carrier lifetime. Generally, the carrier diffusion of heterojunction devices generates built-in potential ( $V_{bi}$ ) under thermal equilibrium conditions [39]. It is well-known that a higher  $V_{bi}$  means a stronger electric field to separate the electron-hole pairs for a higher open-circuit voltage ( $V_{OC}$ ). The capacitance–voltage ( $C$ - $V$ ) relationship follows the Mott–Schottky equation. The Mott–Schottky curves are present in Fig. 4b, and the target device shows a higher  $V_{bi}$  (1.01 V) than the control device (0.89 V). The  $V_{OC}$  response under different light intensities was further used to evaluate carrier recombination. The relationship between the  $V_{OC}$  and light intensity is plotted in Fig. 4c, and the ideality factor ( $n$ ) can be calculated via the following equation [38]:

$$V_{OC} = n \left( \frac{k_B T}{q} \right) \ln(I) + C$$

where  $q$ ,  $T$ ,  $k_B$ , and  $C$  stand for the elementary charge, temperature, Boltzmann constant, and constant. It is found that the control device shows a slope of  $1.86 k_B T/q$ , while the target device exhibits a lower slope of  $1.25 k_B T/q$ . Generally, the  $n = 1$  indicates a trap-free condition, while the  $n$  over 1 suggests the existence of defect-induced non-radiative recombination. Lower  $n$  suggested that the bulk and surface trap-assisted non-radiative recombination is observably restrained [39,40]. Fig. 4d displays the dark  $J$ - $V$  curves without or with BH modification. Compared with the control device, the target device exhibits a smaller current leakage, which indicates that the charge transfer is improved and the charge recombination loss is reduced after the modification of BH. In a word, the carrier dynamics of the device are significantly improved after the BH modification.

As reported, the  $I^-$  in the precursor solution is easily oxidized to notorious  $I_2$ , which can affect the PSC's PCE and stability severely. Fig. 5a presents the DMF solution of iodine without and with BH. It is well-known that an iodine solution usually appears dark red. For the control device, after 2 min, the color of the solution is still not changed. While for the target device, the solution was dark red at first, and then gradually faded, and the final solution color was

**Fig. 3.** (a) Photoluminescence and (b) photoluminescence time-resolved spectra of the perovskite films with the structure of a glass/perovskite or glass/perovskite + benzoyl hydrazine (BH), which were measured from the perovskite side, photoluminescence mapping images of the perovskite films (c) without or (d) with BH modification. Dark  $J$ - $V$  curves of the electron-only devices with the structures of (e) FTO/TiO<sub>2</sub>/perovskite/PCBM/Ag and (f) FTO/TiO<sub>2</sub>/perovskite + BH/PCBM/Ag. The hole-only devices with the structures of (g) FTO/PEDOT:PSS/perovskite/Spiro-OMeTAD/Ag and (h) FTO/PEDOT:PSS/perovskite + BH/Spiro-OMeTAD/Ag.

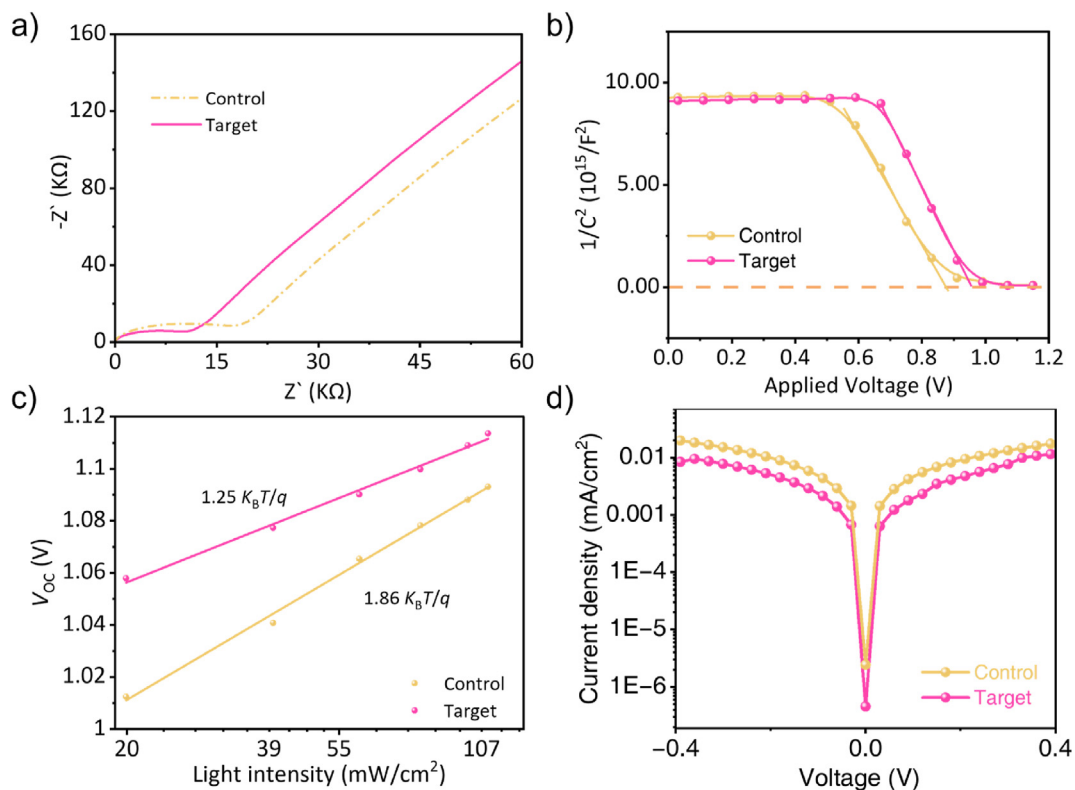


**Fig. 4.** (a) Nyquist plots of the control and target devices measured at a bias of 0 V in the dark. (b) Mott–Schottky plots for the control and target devices. The  $V_{bi}$  is determined by the voltage intercept of  $1/C^2$  curves. (c) The  $V_{OC}$  depends on light intensity for the devices without or with benzoyl hydrazinemodification. (d) Dark  $J-V$  curves of the control and target device.

nearly colorless. The obvious color change indicates that the  $I_2$  can be reduced to  $I^-$  by BH. Therefore, BH can be used to reduce the inevitable generation of  $I_2$  in the precursor. The possible reduction reactions that occur in the precursor are shown in Fig. S4, [25]. The XPS result of N 1s presented in Fig. 1f also proves the reduction reactions. For the target device, a small XPS peak can be seen at 402.21 eV, which is referred to  $-N^+$ , while the peak cannot be obvious in the control film [41]. In addition, BH is also expected to inhibit the  $I^-$  migration in the film due to there indeed being a strong chemical interaction between BH and perovskite as supported by XPS. So, UV–vis was further performed to evaluate the inhibition of  $I^-$  migration. As reported in our previous work, the generation of  $I_2$  is usually accompanied by the migration and reaction of  $I^-$  by the following reactions:  $I^- + I^- \rightarrow I_2$ . Therefore,  $I^-$  migration can be assessed indirectly by evaluating the content of  $I_2$  in a toluene solution [24,25]. As presented in Fig. 5b, after soaking the perovskite film in a toluene solution for 48 h, a clear absorption peak of  $I_2$  located at 500 nm was observed for the control film, while no absorption peak of  $I_2$  is observed at 500 nm in the target film. This can mainly be attributed to the strong chemical interaction between BH and perovskite, which block the migration path of  $I^-$ .

The improved film quality and suppressed interfacial charge recombination by BH modification encouraged us to further uncover the effect of BH modification on device performance. The effect of BH concentrations on device performance is compared and exhibited in Table S2, Fig. 5c, and Fig. S5, the concentrations achieving the optimal photovoltaic performance were 0.25 mg/mL for BH. After treatment with BH, all of the photovoltaic parameters are improved. The average  $V_{OC}$  was increased from  $1.081 \pm 0.0065$  V for the control devices to  $1.103 \pm 0.0048$  V for the target devices. Meanwhile, the average FF was increased from  $78.63 \pm 0.3335$  for

the control devices to  $81.3 \pm 0.2096$  for the target devices. The increased  $V_{OC}$  and FF can be attributed to the following aspects: 1) the decreased film defects can be seen in PL and space charge limited current. 2) Less interfacial non-radiative recombination supported by PL and TRPL. 3) Suppressed ion migration due to the strong chemical interaction between the BH and perovskite film. 4)  $I_2$  was reduced to  $I^-$  due to the reducibility of  $-NH-NH_2$  in BH. The average  $J_{SC}$  was increased from  $24.68 \pm 0.0013$   $mA/cm^2$  of the control devices to  $25.16 \pm 0.0009$   $mA/cm^2$  of the target devices, which can be owing to the increased thickness of the perovskite film increasing the light absorption. As a result of improved  $V_{OC}$ , FF, and  $J_{SC}$ , the average PCE was increased from  $20.99 \pm 0.1527$  (control) to  $22.62 \pm 0.0909$  (target).

The  $J-V$  curves of the devices without and with BH modification are exhibited in Fig. 5d and the corresponding photovoltaic parameter are listed in Table S2. The PCE of the champion device was increased from 21.11% for the control device ( $V_{OC} = 1.08$  V, FF = 78.75, and  $J_{SC} = 24.82$   $mA/cm^2$ ) to 22.75% for the target device ( $V_{OC} = 1.11$  V, FF = 81.26, and  $J_{SC} = 25.22$   $mA/cm^2$ ). To evaluate the effect of BH on the precursor solution of the perovskite, we placed the precursor solution for 72 h and then prepared it into corresponding devices. The  $J-V$  curves are observed and plotted in Fig. S6 and the photovoltage parameter is listed in Table S3. As we can see that after a long time the devices based on the BH-modified precursor solution still exhibited a high PCE (FS: 22.16%, RS: 22.40%), while the control device show a poor PCE (FS: 16.19%, RS: 16.31%), the significant difference further proves the benefit of BH. The incident photon-to-current conversion efficiency spectra in Fig. 5e were further employed to evaluate the current. The integrated current densities were 24.13  $mA/cm^2$  for the control device and 24.96  $mA/cm^2$  for the target device, which is similar to the result of the  $J-V$  curves. Increased integrated current densities can be owing

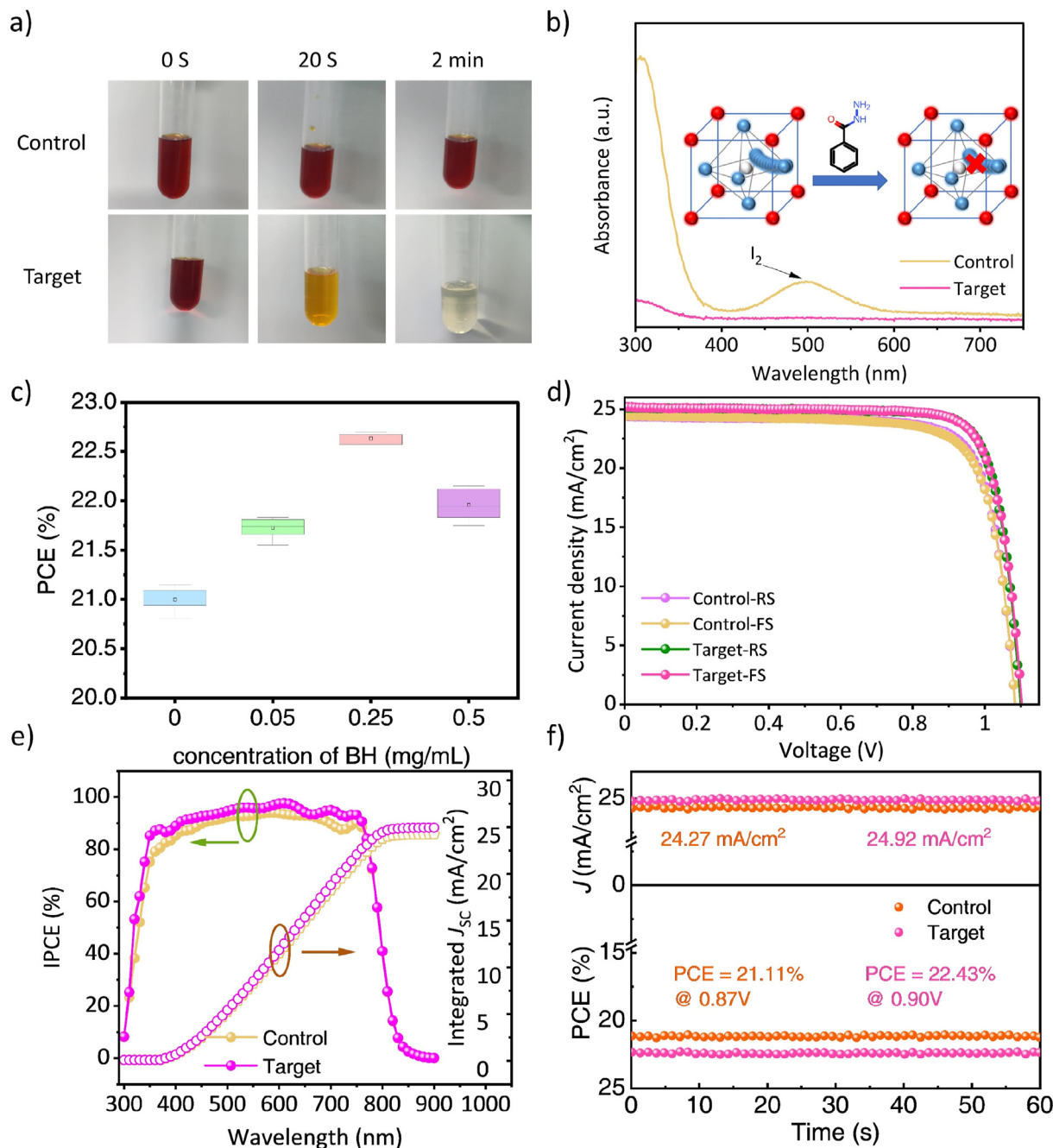


**Fig. 5.** (a) Photographs of the  $I_2$  solutions without (Control) and with the benzoyl hydrazine (BH) (Target) additive with different aging times. (b) Ultraviolet–visible absorption spectra of the toluene solutions dissolved with the perovskite film with and without BH modification, the inset is a schematic diagram of ion migration. (c) Statistical distributions of the power conversion efficiency of the perovskite solar cell treated with different concentrations of BH. (d)  $J$ - $V$  curves of the champion device, (e) incident photon-to-current conversion efficiency curves, and (f) stabilized power conversion efficiencies and the photocurrent density at maximum power point with and without BH modification.

to the increased thickness of the perovskite film after introducing BH. The steady-state output current density and PCE for the control and target PSCs at the maximum power point (MPP) under one sun illumination for 60 s are presented in Fig. 5f. Obviously, the PCE was increased from 21.11% ( $V_{MPP} = 0.87$  V, control) to 22.43% ( $V_{MPP} = 0.90$  V, target). Besides, photo-response curves were carried out to assess the film quality. As exhibited in Fig. 6a and b, the curve control film shows a slope of 0.017, while the target film exhibits a slope of 0.021. The larger curve slope supports a more sensitive light response, which can be attributed to better film

quality. All in all, all the photovoltaic parameters were improved after the BH modification.

Expect for the PCE, the stability of the device is another key factor that affects the commercialization of PSCs. Therefore, we further judged the stability of the unencapsulated devices with or without BH modification under different conditions. First, the device was put in an air and dark condition (25 °C, 5–10% RH) (Fig. 6c and Fig. S7). After aging for 500 h, the control device degraded 8% of its original PCE, while the BH-treated devices only degraded 2%. For the humidity test, the device was put into a relative humidity of 40–50%

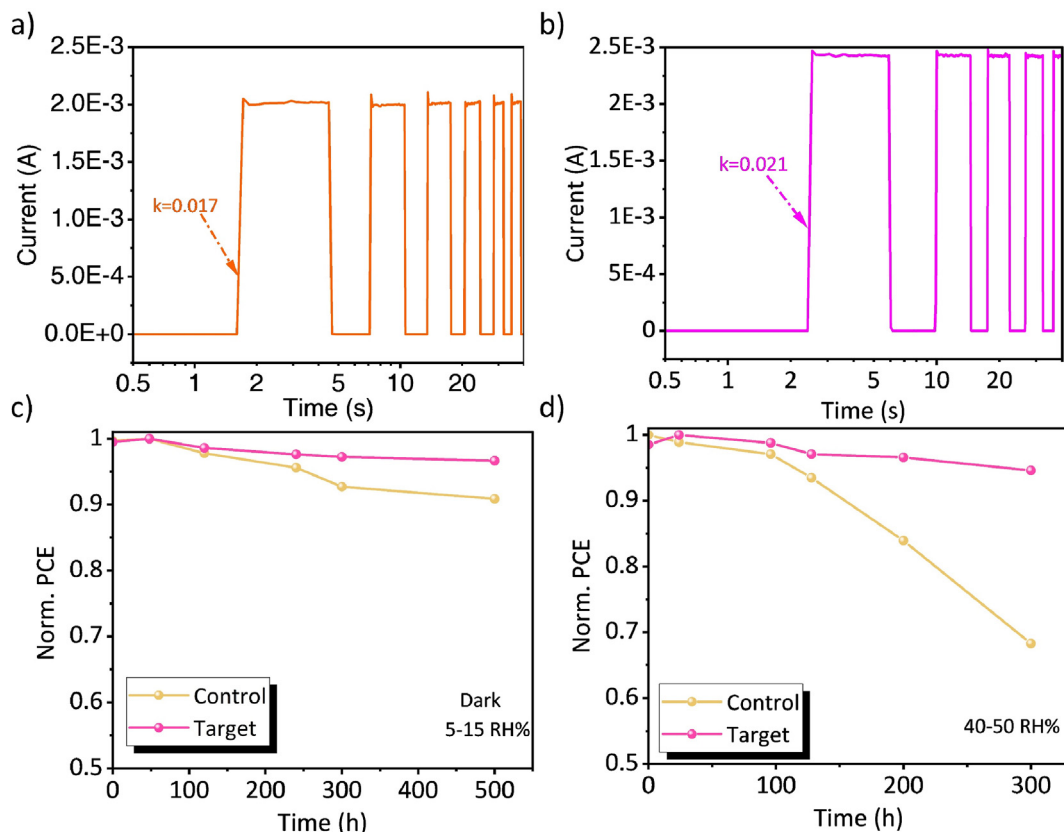


**Fig. 6.** The light response curve of (a) the control and (b) the target device. (c) Stability in the air condition of the unsealed control and target devices aged in the dark. (d) The humidity stability of the device without and with benzoyl hydrazine modification aged in air condition.

and the results are listed in Fig. 6d and Fig. S8. After 300 h, the PCE of the target device still maintains 94.6% of its initial PCE, while the control device degrades to 68.2% of its initial PCE. For the comprehensive test, the devices were put into a hot plate at 65 °C and natural light air conditioners with a 15–25% RH. As displayed in Fig. S9, the PCE of the target device maintains 96.8% of its original after 100 h, while the control device only keeps its initial PCE of 73.8%. Finally, Fig. S10 exhibits the photostability of the devices with and without BH modification aged in a N<sub>2</sub>-filled glovebox under one sun illumination and room temperature condition. After aging for 100 h, the PCE of the control device degraded to 90% of its initial value, while the PCE of the device with BH degraded to 95% of its initial value, indicating enhanced photostability by BH. In a word, the stabilities of the device were increased after the modification of BH. It has been widely reported that the trap-assisted non-radiative recombination and I<sup>-</sup> migration would accelerate the degradation of PSCs. Consequently, improved stability should be primarily due to the reduced defect density, inhibited I<sup>-</sup> migration, and suppressed trap-assisted non-radiative recombination.

### 3. Conclusions

In summary, we have introduced a new additive of BH into the perovskite precursor solution to passivate the defects in the perovskite absorber film. The mechanism to enhance the device's performance and stability was systematically investigated. Fourier transform infrared spectroscopy and XPS supported that the C=O group in BH could repair the uncoordinated Pb<sup>2+</sup> in the film through coordination bonds, while the Lewis base-acid adduct formed by the interaction of C=O and Pb<sup>2+</sup> further improves the crystallization of the perovskite. Additionally, the weak interaction

between the BH and perovskite film cannot only inhibit the migration of I<sup>-</sup> but also prevent the movement of cations to reduce cation vacancies. Meanwhile, BH can stabilize the precursor solution by hindering the generation of I<sub>2</sub> in the precursor solution due to its strong reduction ability. Finally, the BH-optimized PSC achieves an enhanced PCE of 22.75% together with improved stability, demonstrating the multifunction of BH molecules. These results confirm that the addition of BH is a facile and practical approach for obtaining highly efficient and stable PSCs. This work could contribute in accelerating the industrialization of perovskite optoelectronic devices.

### Credit author statement

**Huan Bi:** conceptualization, validation, investigation, writing – original draft, and writing – review & editing.

**Mengna Guo:** validation.

**Chao Ding:** validation and formal analysis.

**Shuzi Hayase:** supervision.

**Qing Shen:** validation, resources, supervision, and project administration.

**Gaoyi Han:** validation, resources, supervision, and funding acquisition.

**Wenjing Hou:** validation, resources, writing – review & editing, supervision, and funding acquisition.

### Declaration of competing interest

The authors declare that they have no known competing financial interests or personal relationships that could have appeared to influence the work reported in this paper.

## Data availability

Data will be made available on request.

## Acknowledgments

This work was financially supported by the National Natural Science Foundation of China (61804091, and U21A6004), Scientific and Technological Innovation Programs of Higher Education Institutions in Shanxi (2020L0002), and the Natural Science Foundation of Shanxi Province under Grant (201901D211127), Program of State Key Laboratory of Quantum Optics and Quantum Optics Devices (No: KF201910). We are grateful for the Scientific Research Start-up Funds of Shanxi University and the Hundred Talents Plan of Shanxi Province. This research was partly supported by the Japan Science and Technology Agency (JST) Mirai program (JPMJMI17EA). We also would like to thank Shiyanjia Lab ([www.shiyanjia.com](http://www.shiyanjia.com)) for the support of XPS tests.

## Appendix A. Supplementary data

Supplementary data to this article can be found online at <https://doi.org/10.1016/j.mtener.2023.101269>.

## References

- [1] A. Kojima, K. Teshima, Y. Shirai, T. Miyasaka, *J. Am. Chem. Soc.* 131 (2009) 6050–6051.
- [2] H. Bi, Y. Guo, M. Guo, C. Ding, S. Hayase, T. Mou, Q. Shen, G. Han, W. Hou, *Chem. Eng. J.* 439 (2022), 135671.
- [3] H. Min, D.Y. Lee, J. Kim, G. Kim, K.S. Lee, J. Kim, M.J. Paik, Y.K. Kim, K.S. Kim, M.G. Kim, T.J. Shin, S. Il Seok, *Nature* 598 (2021) 444–450.
- [4] G. Kim, H. Min, K.S. Lee, D.Y. Lee, S.M. Yoon, S.I. Seok, *Science* 370 (2020) 108–112.
- [5] H. Wang, C. Zhu, L. Liu, S. Ma, P. Liu, J. Wu, C. Shi, Q. Du, Y. Hao, S. Xiang, H. Chen, P. Chen, Y. Bai, H. Zhou, Y. Li, Q. Chen, *Adv. Mater.* 31 (2019), 1904408.
- [6] NREL, Best Research-Cell Efficiency Chart, 2021. <https://www.nrel.gov/pv/cell-efficiency.html>.
- [7] S.N. Habisreutinger, D.P. McMeekin, H.J. Snaith, R.J. Nicholas, *Apl. Mater.* 4 (2016), 091503.
- [8] B. Conings, J. Drijkoningen, N. Gauquelin, A. Babayigit, J. D'Haen, L. D'Olieslaeger, A. Ethirajan, J. Verbeeck, J. Manca, E. Mosconi, F.D. Angelis, H.-G. Boyen, *Adv. Energy Mater.* 5 (2015), 1500477.
- [9] E.J. Juarez-Perez, Z. Hawash, S.R. Raga, L.K. Ono, Y. Qi, *Energy Environ. Sci.* 9 (2016) 3406–3410.
- [10] S.-H. Turren-Cruz, A. Hagfeldt, M. Saliba, *Science* 362 (2018) 449–453.
- [11] A. Mahapatra, D. Prochowicz, M.M. Tavakoli, S. Trivedi, P. Kumar, P. Yadav, *J. Mater. Chem.* 8 (2020) 27–54.
- [12] F. Zhang, K. Zhu, *Adv. Energy Mater.* 10 (2020), 1902579.
- [13] S. Liu, Y. Guan, Y. Sheng, Y. Hu, Y. Rong, A. Mei, H. Han, *Adv. Energy Mater.* 10 (2020) 345–351.
- [14] D. Yang, Y. Weng, Z. Shen, M. Jin, H. Shen, Q. Du, J. Zheng, F. Li, C. Chen, *Chem. Eng. J.* 454 (2023), 140160.
- [15] W. Wang, Q. Zhou, D. He, B. Liu, L. Bai, C. Xu, Q. Song, P. Zhao, C. Chen, K. Sun, H. Yang, Z. Zang, D. Lee, J. Chen, *Sol. RRL* 6 (2022), 2100893.
- [16] Z. Ma, W. Zhou, D. Huang, Q. Liu, Z. Xiao, H. Jiang, Z. Yang, W. Zhang, Y. Huang, *ACS Appl. Mater.* 12 (2020) 52500–52508.
- [17] S. Chen, X. Dai, S. Xu, H. Jiao, L. Zhao, J. Huang, *Science* 373 (2021) 902–907.
- [18] E. Bi, Z. Song, C. Li, Z. Wu, Y. Yan, *Trends Chem* 3 (2021) 575–588.
- [19] Y. Zhao, W. Zhou, Z. Han, D. Yu, Q. Zhao, *Phys. Chem. Chem. Phys.* 23 (2021) 94–106.
- [20] Y. Yuan, J. Huang, *Acc. Chem. Res.* 49 (2016) 286–293.
- [21] J.M. Azpiroz, E. Mosconi, J. Bisquert, F. De Angelis, *Energy Environ. Sci.* 8 (2015) 2118–2127.
- [22] Y. Du, S. Wan, M. Xie, Y. Xia, W. Yang, Z. Wei, Y. Zhu, Y. Hua, Z. Jin, D. Hong, Y. Tian, *J. Phys. Chem. Lett.* 12 (2021) 7106–7112.
- [23] Y. Zhou, Y. Yin, X. Zuo, L. Wang, T.-D. Li, Y. Xue, A. Subramanian, Y. Fang, Y. Guo, Z. Yang, M. Cotlet, C.-Y. Nam, M.H. Rafailovich, *Chem. Mater.* 33 (2021) 6120.
- [24] M. Yang, G. Han, Y. Xiao, W. Hou, *Chem. Commun.* 58 (2022) 5638–5641.
- [25] S. Chen, X. Xiao, H. Gu, J. Huang, *Sci. Adv.* 7 (2021), eabe8130.
- [26] H. Bi, B. Liu, D. He, L. Bai, W. Wang, Z. Zang, J. Chen, *Chem. Eng. J.* 418 (2021), 129375.
- [27] X. Zuo, B. Kim, B. Liu, D. He, L. Bai, W. Wang, C. Xu, Q. Song, C. Jia, Z. Zang, D. Lee, X. Li, J. Chen, *Chem. Eng. J.* 431 (2021), 133209.
- [28] H. Bi, X. Zuo, B. Liu, D. He, L. Bai, W. Wang, X. Li, Z. Xiao, K. Sun, Q. Song, Z. Zang, J. Chen, *J. Mater. Chem.* 9 (2021) 3940–3951.
- [29] Q. Jiang, Y. Zhao, X. Zhang, X. Yang, Y. Chen, Z. Chu, Q. Ye, X. Li, Z. Yin, J. You, *Nat. Photonics* 13 (2019) 460–466.
- [30] S.N. Kumar, G. Bouyssoux, F. Gaillard, *Surf. Interface Anal.* 15 (1990) 531–536.
- [31] L. Wang, X. Wang, L. Zhu, S.-B. Leng, J. Liang, Y. Zheng, Z. Zhang, Z. Zhang, X. Liu, F. Liu, C.-C. Chen, *Chem. Eng. J.* 430 (2022), 132730.
- [32] A. Scheludko, B.V. Toshev, D.T. Bojadjev, *J. Chem. Soc., Faraday Trans. 1: Physical Chemistry in Condensed Phases* 72 (1976) 2815–2828.
- [33] X. Guo, B. Zhao, K. Xu, S. Yang, Z. Liu, Y. Han, J. Xu, D. Xu, Z. Tan, S. Liu, *Small* 17 (2021), 2102272.
- [34] Q. Cao, T. Wang, J. Yang, Y. Zhang, Y. Li, X. Pu, J. Zhao, H. Chen, X. Li, I. Tojiboyev, J. Chen, L. Etgar, X. Li, *Adv. Funct. Mater.* 32 (2022), 2201036.
- [35] K. Wang, B. Yu, C. Lin, R. Yao, Z. Nie, H. Wang, H. Yu, *Sol. RRL* 6 (2022), 2200862.
- [36] P. Wang, J. Liu, W. Shang, T. Xu, M. Wang, Y. Shi, R. Cai, J. Bian, *J. Phys. Chem. Lett.* 14 (2023) 653–662.
- [37] L. Xie, J. Chen, P. Vashishtha, X. Zhao, G.S. Shin, S.G. Mhaisalkar, N.-G. Park, *ACS Energy Lett.* 4 (2019) 2192–2200.
- [38] J. Chen, X. Zhao, S.G. Kim, N.G. Park, *Adv. Mater.* 31 (2019), 1902902.
- [39] Q. Lou, H. Li, Q. Huang, Z. Shen, F. Li, Q. Du, M. Jin, C. Chen, *Eco. Mat.* 3 (2021), e12099.
- [40] J. Chen, N.G. Park, *Adv. Mater.* 31 (2019), 1803019.
- [41] B. Lindberg, *Chem. Scr.* 7 (1975) 155–166.